Journal of Materials Chemistry A

COMMUNICATION

View Article Online
View Journal | View Issue

Cite this: J. Mater. Chem. A, 2014, 2, 8190

Received 21st January 2014
Accepted 27th March 2014

DOI: 10.1039/c4ta00365a

www.rsc.org/MaterialsA

Graphene nanocluster decorated niobium oxide nanofibers for visible light photocatalytic applications†

Shishun Qi,‡[ab] Linfeng Fei,‡[b] Ruzhong Zuo,*[a] Yu Wang*[b] and Yucheng Wu[a]

In this paper, we report a novel nanocomposite of graphene nanocluster decorated Nb_2O_5 nanofibers. With the structural modification, the photocatalytically active region of Nb_2O_5 has been significantly extended from the UV region to the UV-Vis region (from ~380 nm to ~800 nm in the adsorption edge); and hence, the visible light photocatalytic performance has been greatly improved. Detailed structural analysis revealed that the enhanced photocatalytic activity of the graphene nanocluster decorated Nb_2O_5 nanofibers could be mainly attributed to the modification of the bandgaps by the clusters and the unique orientation of graphene layers (nearly perpendicular to the Nb_2O_5/C interface, which is quite different from classical "core–shell" composites). We believe that the findings suggest a potential candidate for visible-light photocatalytic applications and would inspire further studies.

Introduction

Worldwide efforts have been made to develop high-performance photocatalytic materials for energy and environmental applications, and titania (TiO_2) is probably the most widely investigated photocatalyst so far. Due to its wide bandgap, TiO_2 is active in the ultraviolet (UV) light range but relatively inert to visible light.[1–4] In order to fully utilize solar energy for photocatalysis, researchers attempted to enhance the visible light photocatalytic activity of TiO_2 through doping, dye sensitization, bandgap engineering, *etc.*[5–11] Among these methods, the use of sensitization could effectively extend the absorption spectrum of TiO_2 at a relatively low cost and is therefore considered to be a promising approach for its large-scale applications.[9–11] Functional carbonaceous materials have been utilized to improve the photocatalytic activity of various materials.[12–15] Recently, graphene has been found to exhibit a high level of absorption in the visible-light region and enhance charge separation along the interfaces between photocatalysts and organic pollutants.[16–20]

Despite the success mentioned above, there is also growing interest in developing material systems other than TiO_2 for photocatalytic applications. For example, with a bandgap (E_g) of 3.4 eV, niobium oxide (Nb_2O_5) is a major semiconductor with great potential for water treatments.[21–25] One of the main advantages of Nb_2O_5 is that it shows long-term stability in a photocatalytic process.[23] Analogous to TiO_2, Nb_2O_5 displays poor photocatalytic activity to visible light due to its large bandgap.[26–28] This issue could be partially solved by carbon modification in Nb_2O_5 nanoplates through a solvothermal method.[28] Nevertheless, there is still much room for enhancing the performance of Nb_2O_5 for photocatalytic applications.

In light of the situation discussed above, we propose to develop a new system – Nb_2O_5 nanofibers (Nb_2O_5 NFs) decorated with graphene nanoclusters. We chose to work on Nb_2O_5 nanofibers rather than nanoparticles mainly because of their better handleability.[29,30] Electrospinning was employed as a feasible and scalable technique in terms of synthesizing submicrometer-sized fibers by utilizing an electrical charge to draw fibers from a liquid with suitable viscosity.[31,32] Graphene, the two-dimensional macromolecular sheet of carbon, exhibits superior electrical conductivity, mechanical properties and large theoretical specific surface areas.[33,34] The introduction of graphene for decorating the surface of Nb_2O_5 nanofibers should improve the nanofibers' photocatalytic activity through (1) visible light absorption originating from the graphene; (2) enhancement of the charge separation because of the formed conjugated structure.

Herein, we report a successful attempt for the fabrication of graphene nanocluster decorated Nb_2O_5 nanofibers *via* a simple electrospinning technique plus a hydrothermal method. As demonstrated in the paper, the material exhibits a significantly extended adsorption spectrum and hence greatly enhanced photocatalytic activity. A possible mechanism for explaining the

[a]School of Materials Science and Engineering, Hefei University of Technology, Anhui 230009, China. E-mail: piezolab@hfut.edu.cn

[b]Department of Applied Physics and Materials Research Center, The Hong Kong Polytechnic University, Hong Kong SAR, China. E-mail: yu.wang@polyu.edu.hk

† Electronic supplementary information (ESI) available. See DOI: 10.1039/c4ta00365a

‡ S.S. Qi and L.F. Fei have made equal contribution to this work.

visible light activity is also proposed based on the detailed structural analysis of the composite nanofibers.

Experimental methods

The samples were prepared *via* an electrospinning process plus a hydrothermal treatment. The precursor solution for electrospinning was prepared by adding 9 wt% polyvinylpyrrolidone (PVP) into a 0.1 mol L^{-1} niobium ethoxide solution followed by stirring for several hours at room temperature.[35] The electrospinning parameters were: distance between the needle and the collector (Al foil) = 14 cm, applied voltage = 16 kV, and precursor feeding rate = 1 mL h^{-1}. After electrospinning, the as-spun fibers were first dried in an oven at 100 °C for several hours and then calcined in a muffle furnace at 500 °C for 1 hour in air. Samples thus prepared are Nb_2O_5 nanofibers, hereafter called Nb_2O_5 NFs. 0.1 g Nb_2O_5 NFs together with glucose were then put into a 40 mL Teflon-lined stainless steel autoclave containing 32 mL of deionized water to produce a 0.5 g L^{-1} glucose solution. The mixture was stirred to form a milk-like suspension, sealed and hydrothermally treated at 180 °C for 4 h. After cooling, filtration, washing (using deionized water) and drying in an oven at 80 °C for 2 h, grey samples were obtained. They are actually Nb_2O_5 NFs coated with carbon. A series of samples with glucose concentrations varying from 0 to 30 g L^{-1} were prepared. In this paper, we only discuss two samples prepared with a relatively low glucose concentration (0.5 g L^{-1}) and a higher glucose concentration (30 g L^{-1}).

X-ray diffraction (XRD) measurements were carried out using an XRD diffractometer (XRD, D/Max-RB, Rigaku, Japan) with a Cu Kα line of 0.1541 nm. The morphologies of the as-prepared samples were observed by means of scanning electron microscopy (SEM, SU8020, Hitachi, Japan) and transmission electron microscopy (TEM, JEM-2100F, JEOL, Japan). Ultraviolet-visible (UV-Vis) diffuse reflective spectra were recorded using a UV-Vis spectrometer (TU-1950, Beijing Purkinje General Instrument Co., Ltd, China). The photoluminescence (PL) spectra of the samples were detected using a Jobin Yvon HR 800 micro-Raman spectrometer using the 325 nm line from a He–Cd laser. X-ray photoelectron spectroscopy was accomplished using an X-ray photoelectron spectrometer (XPS, ESCALAB 250, Thermo, America).

The visible light photocatalytic activity of the samples was evaluated by degradation of methyl orange (MO) (at the natural pH value) under irradiation of a 400 W metal-halide lamp equipped with a cut-off glass filter transmitting $\lambda > 380$ nm. The quartz reaction vessel was cooled by the circling water. For the degradation of MO, the initial concentration of MO was 20 mg L^{-1} with a photocatalyst loading of 1 g L^{-1}. First, the solution was stirred in the dark to reach an adsorption–desorption equilibrium between the organic molecules and the catalyst. Upon irradiation for a certain time interval, a small amount of the solution was taken and centrifuged; the concentration of MO was determined by measuring its absorbance at 464 nm.

Results and discussion

Microstructures of all samples were carefully examined through XRD, SEM and TEM. Fig. 1a shows the typical SEM image of the hydrothermally treated Nb_2O_5 nanofibers, which are ~200 nm in diameter and a few to several tens of micrometers in length. As shown in Fig. 1b, the XRD measurement indicates that all samples are well crystallized with a hexagonal structure, matching well with the database (JCPDS no. 28-0317). The XRD pattern of the sample after hydrothermal treatment is basically the same as that before the treatment. No diffraction peak was identified to belong to carbon (which should be located at $2\theta = 25.6°$) due to its low percentage.[36]

The high resolution TEM (HRTEM) analysis then revealed that the morphology and structure of the carbon coating on Nb_2O_5 NFs are highly dependent on the concentration of glucose in the hydrothermal step. The sample prepared with a low glucose concentration (0.5 g L^{-1}) was found to have discontinuous graphene nanoclusters formed on the surface of Nb_2O_5 NFs, as shown in Fig. 1c to e. The fringes of the nanocluster implied that carbon was partially crystallized with a *d*-spacing of ~0.34 nm, which matched well with typical data for the interlayer distance in graphite.[10] The Nb_2O_5 NFs were well crystallized and composed of uniform nanograins. The corresponding lattice fringe was 0.24 nm, agreeing well with the lattice spacing of the $(1\bar{1}01)$ planes of hexagonal Nb_2O_5. On the basis of the structural features discussed above, this sample is hereafter called G@Nb_2O_5 NFs, meaning graphene nanocluster decorated Nb_2O_5 NFs.

For samples prepared with higher glucose concentration (30 g L^{-1}), continuous and uniform graphite layers with a total thickness of ~4 nm are found on the surface of Nb_2O_5 NFs, forming a typical core–shell structure, as shown in Fig. 1f and g. This sample is called C@Nb_2O_5 NFs, meaning carbon layer coated Nb_2O_5 nanofibers. It should be noted that the

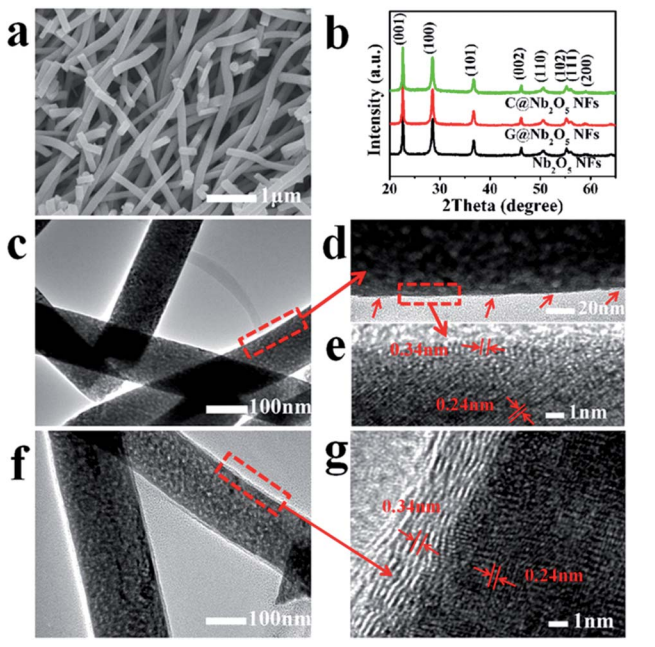

Fig. 1 (a) SEM image of sample G@Nb_2O_5 NFs. (b) XRD patterns of Nb_2O_5 NFs, G@Nb_2O_5 NFs and C@Nb_2O_5 NFs. (c–e) TEM image of G@Nb_2O_5 NFs, enlarged TEM image and HRTEM image of G@Nb_2O_5 NFs. (f and g) TEM and HRTEM images of C@Nb_2O_5 NFs.

orientation of the graphene layers varied with carbon percentage. For G@Nb_2O_5 NFs, the carbon existed in the form of graphene nanoclusters with graphene layers lying almost vertical to the axial direction of Nb_2O_5 nanofibers. In contrast, for the C@Nb_2O_5 NFs, carbon existed in the form of continuous coating layers, which was parallel to its axial direction of the Nb_2O_5 nanofibers. HR-TEM analyses were also conducted for the samples prepared at intermediate glucose concentrations (shown in Fig. S1†). The images displayed the evolution of a carbon layer from discontinuous thin layers consisting of randomly oriented "sheets" to continuous coated layers with the same orientation.

To further understand the roles played by the graphene nanocluster in the composited fibres, optical absorption properties of the samples were examined using a UV-Vis spectrometer. As shown in Fig. 2a, the bare Nb_2O_5 nanofibers exhibit poor absorption of visible light and the absorption edge is ~380 nm, corresponding to a bandgap of 3.4 eV (inset of Fig. 2a). The G@Nb_2O_5 NFs and C@Nb_2O_5 NFs, however, exhibited much higher visible light absorption up to a wavelength of 800 nm, suggesting much narrowed bandgaps, and the bandgap values were determined to be 3.1 eV and 2.9 eV, respectively. The absorption enhancement could be caused by the fact that carbon could absorb visible light and that the improved synergistic effect may have been a result of the joint electronic system at the interface formed between Nb_2O_5 and carbon.[9,19] Moreover, it has also been reported that graphene nano-ribbons could form a bandgap.[37,38] Herein, the clusters were in such a small size that a bandgap might be formed and it would be partially responsible for the visible light absorption in G@Nb_2O_5. The visible light photocatalytic activities of all samples were examined through measuring the degradation rate of MO (represented by the ratio C/C_0, where C and C_0 stand for the remnant and initial concentration of MO) in the presence of the nanofibers under visible light irradiation with wavelength λ > 380 nm. To make the results reliable, control experiments were firstly conducted under different conditions: (1) in the presence of the photocatalyst but without the light irradiation and (2) with visible light irradiation but in the absence of a photocatalyst. As shown in Fig. 2b, the experiments reveal that there is no appreciable decrease of the MO concentration over the samples after the first 30 min, indicating an adsorption–desorption equilibrium of MO. Besides, a small reduction of the MO concentration about 5% could be observed after the visible light irradiation for 5 h, confirming the negligible photodegradation in the system. The results of the photocatalytic experiments are shown in Fig. 2c. Bare Nb_2O_5 NFs displayed poor visible-light photocatalytic activity (degradation efficiency of ~20% for 5 h) due to the relatively large band gap.[35] Samples with carbon decoration showed a much higher visible-light photocatalytic activity: degradation efficiencies of ~95% for G@Nb_2O_5 NFs and ~65% for C@Nb_2O_5 NFs. It is interesting to note that G@Nb_2O_5 NFs showed the highest efficiency despite their low carbon concentration. Photocatalytic experiments were also conducted for the samples prepared at intermediate concentrations and the results are clearly displayed in Fig. S2,† indicating that the photocatalytic activity was closely related to the state of the deposited carbon. Therefore, it is clear that graphene nanoclusters and discontinuous carbon layers were beneficial for obtaining higher degradation efficiency. Comparing the efficiency of samples obtained at 10 g L^{-1}, 20 g L^{-1} and 30 g L^{-1}, it could be seen that a slight increase of the carbon content would result in an obvious decrease in the degradation capacity. Fig. 2d shows $-\ln(C/C_0)$ *vs.* reaction time profiles for the three samples. According to the results, the photocatalytic reaction constant k was 0.5470 h^{-1} for G@Nb_2O_5 NFs, which was almost three times more than that of C@Nb_2O_5 NFs (k = 0.1950 h^{-1}). G@Nb_2O_5 NFs exhibited much higher efficiency than that of C@Nb_2O_5 NFs. This was closely related to the feature of graphene nanoclusters which was different from the continuous carbon layers on the C@Nb_2O_5 NFs. Cycling experiments were also conducted for G@Nb_2O_5 NFs and C@Nb_2O_5 NFs. The obtained results are displayed in Fig. S3.† It could be detected that C@Nb_2O_5 NFs exhibited almost no changes in the degradation efficiency after three cycling experiments, while a slight decrease of about 5% was observed for the G@Nb_2O_5 NFs in the second and third run. However, the degradation efficiency of G@Nb_2O_5 NFs was still much higher than that of C@Nb_2O_5 NFs. The favourable photocatalytic activity of our sample was comparable with previous reports for similar systems like TiO_2, ZnO and CdS, showing great potential as a promising visible light photocatalyst.[19,39–41] Due to the limit of the relatively large diameter of the composite nanofibers, the efficiency was lower than some systems with much smaller dimensions, such as RGO–CdS nanorods, RGO–ZnO nanoparticles, C–$Bi_{12}TiO_{20}$ nanorods and G–SnO_2 aerosol.[42–45] Detailed information can be seen in Table SI (ESI†).

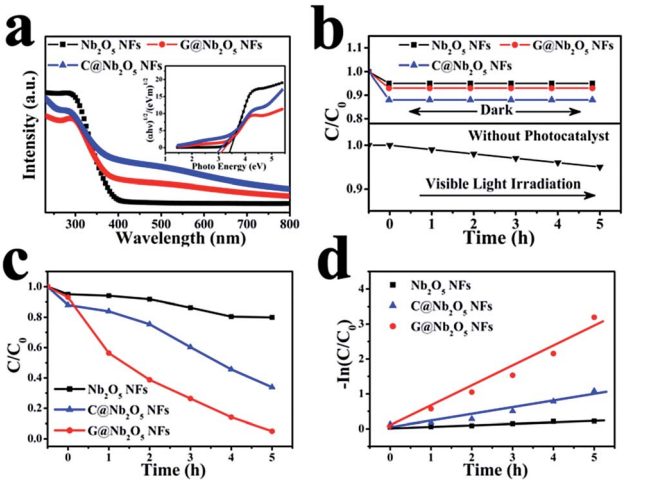

Fig. 2 (a) UV-Vis absorption spectra of the three samples. (b) Degradation profiles of MO in the presence of the G@Nb_2O_5 NFs and C@Nb_2O_5 NFs but in the dark, and with visible light irradiation but in the absence of the nanofiber photocatalysts. (c) Photocatalytic degradation profiles of MO over the three samples. (d) Kinetic linear simulations of MO photocatalytic degradation among different samples.

To better understand the aforementioned synergistic effect for the enhanced visible light photocatalytic activity, X-ray photoelectron spectroscopy (XPS) analysis was also conducted

to reveal the nature of contact between Nb_2O_5 and carbon. Fig. 3a presents the XPS survey spectra of G@Nb_2O_5 NFs (inset figure) and the enlarged high resolution XPS spectra of the C 1s region around 285 eV. As indicated in the inset spectra, all peaks could be identified to belong to Nb, O and C, suggesting the coexistence of these elements in the samples. For the C 1s region, the binding energy with a peak at 284.5 eV was attributed to the accumulation of graphite carbon.[20,46] In addition to the strong peak at 284.5 eV, two weak peaks were also observed at 285.8 eV and 288.5 eV, representing the characteristic signatures of the carbonate with oxygen bond species C–O and C═O, respectively.[10] Consequently, the XPS results suggested the formation of carbon-modified Nb_2O_5 nanofibers and the coated carbon species functionalized as a surface sensitizer to absorb visible light.[28] The C 1s result for the C–Nb_2O_5 sample exhibited almost no changes, which is not shown here.

To clarify the deep reason for the enhanced activity, the contact issue should also be considered which had always been a key factor in the overall performance of a composite. In a carbon–metallic oxide system, the physicochemical nature of the contact could vary upon different sample preparing methods. For example, in the TiO_2–carbon system, there are generally two kinds of carbon in the composite system. The first kind is doping, which means certain atoms in the TiO_2 lattice are substituted by carbon atoms, thus a new energy band structure is achieved. The second one is surface modification (carbon coating), forming an electronic interaction which was responsible for the sensitization effect.[9,10] In our case, the Nb_2O_5 nanofibers were modified by the surface coated carbon. This structure not only ensures good connection but also helps to separate the photo-generated electrons and holes effectively. Fig. 3b presents the PL spectroscopy of the three samples. As shown in the inset figure, an excitation light with wavelength at 325 nm was chosen and the bare Nb_2O_5 NFs exhibited the highest luminescence intensity, indicating more recombination of the photo-generated electron–hole pairs. By contrast, the recombination of the charge carriers was greatly inhibited in the carbon decorated samples which could be detected from the much lower emission intensity. Besides that, the PL emission intensity decreased with the increase of the thickness of the graphene layers. Therefore, it was reasonable to conclude that effective separation of the photo-generated electron and hole pairs could be achieved by the deposition of graphene layers in vertical and parallel directions.

With the structural information extracted above, mechanisms for the visible photocatalytic behaviour of our samples and the difference of activity between the G@Nb_2O_5 and C@Nb_2O_5 NFs were proposed. As shown in Fig. 4, Nb_2O_5 NFs can only show UV-light photocatalytic activity *via* chemical reactions that would lead to the formation of chemically active radicals (*e.g.* $HO_2^{\bullet}$), a mechanism already well documented. However, after coating Nb_2O_5 with carbon of different morphologies, G@Nb_2O_5 NFs and C@Nb_2O_5 NFs could absorb both UV and visible light, leading to the excitation of carbon and electrons being transferred to the conduction band of the Nb_2O_5, resulting in photocatalytic activity in the visible light region.[9,10,19,20] For our samples, the alignments of carbon layers were closely related to the carbon content. The possible mechanism for the carbon-content dependent photocatalytic performance (shown in Fig. S2†) of the composite can be proposed. On one hand, a higher carbon content would lead to better absorption of visible light and hence, higher photocatalytic activity. On the other hand, however, the continuous carbon layer would reduce the exposure of Nb_2O_5 NFs to the light and

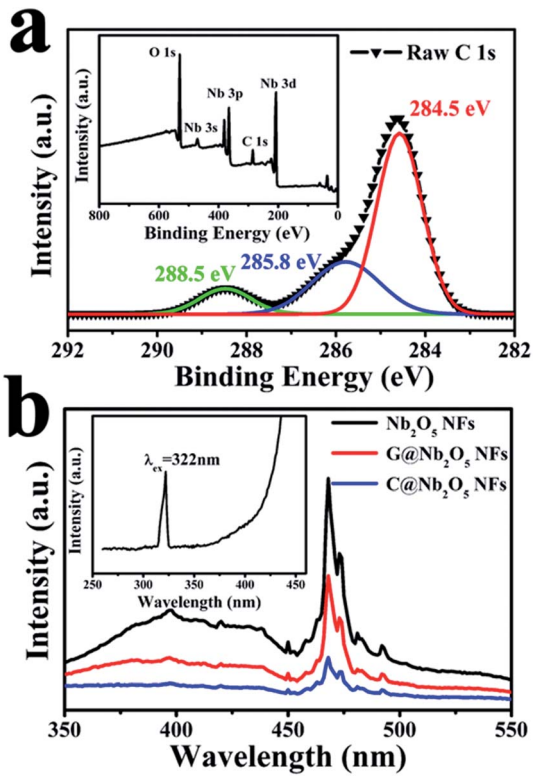

Fig. 3 (a) XPS spectra of C 1s for G@Nb_2O_5 NFs, and the inset figure is the fully scanned spectra. (b) PL spectra for the three samples.

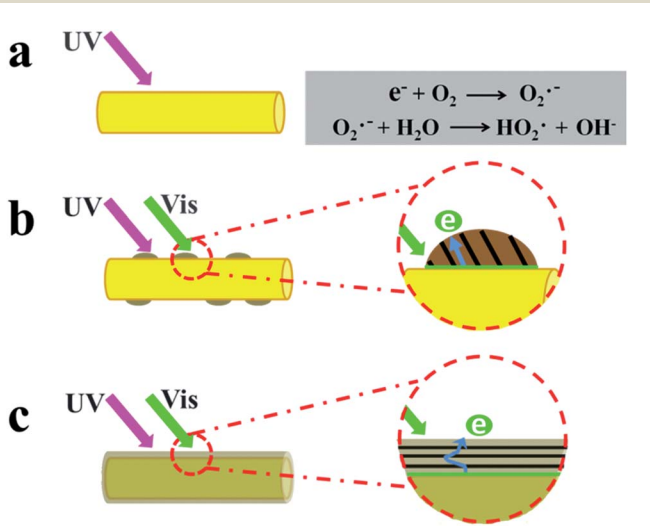

Fig. 4 Proposed mechanisms for the visible light-induced photodegradation of MO by the composite nanofibers.

would result in more barriers for the transfer of optical charges. Such repetition between two controversial effects has also been observed in other composite systems.[8] Apart from this factor, the alignment of the graphite layers was also an important reason why G@Nb_2O_5 NFs exhibited better photocatalytic activity than C@Nb_2O_5 NFs, which is clearly displayed in Fig. 4b and c. It is well known that graphite layers are highly anisotropic materials – the charge mobility along the directions of graphene layers is much larger than that along its normal direction. In G@Nb_2O_5 NFs, graphene nanoclusters grew in such a way that the carbon sheets were nearly vertically aligned to the Nb_2O_5 NFs, while in C@Nb_2O_5 NFs, the carbon sheets were parallel to the Nb_2O_5 NFs. The electrons have to pass through the carbon sheet instead of passing along the sheet to react with the organic pollutant. Moreover, due to the high specific surface area of graphite layers, the MO molecules could be adsorbed on the surface. Thus, the vertically aligned graphene layers on the nanofibers could not only make full use of the excellent in-plane conductivity of graphene, but also promote the effective contacts between MO molecules and the Nb_2O_5/graphene content, leading to the acceleration of the photocatalytic reaction. The carbon-content dependent photocatalytic performance of composite samples prepared at various glucose concentrations (shown in Fig. S2†) could be well explained by the proposed mechanism.

In summary, niobium oxide nanofibers decorated with graphene nanoclusters were successfully synthesized *via* an electrospinning process followed by a hydrothermal treatment. The composite nanofibers displayed a fairly high photocatalytic activity in the visible-light region, which had never been found in pure niobate nanostructures. Through analysis, it was found that G@Nb_2O_5 NFs exhibited favourable features in visible light absorption, charge separation and charge transfer during the photocatalytic process. The discontinuous coverage and nearly vertical alignment of graphite layers in G@Nb_2O_5 NFs were important structural factors leading to a high visible-light photocatalytic activity. Therefore, the graphene nanocluster decorated Nb_2O_5 nanostructures could be potential candidates for applications of eliminating organic pollutants in waste water.

Acknowledgements

This work was financially supported by the National Natural Science Foundation of China (51272060) and the Hong Kong Polytechnic University (A-PK29 and A-PL53).

Notes and references

1 H. Yoneyama, Y. Yamashita and H. Tamura, *Nature*, 1979, **282**, 817–818.
2 R. Asahi, T. Morikawa, T. Ohwaki, K. Aoki and Y. Taga, *Science*, 2001, **293**, 269–271.
3 X. B. Chen and S. S. Mao, *Chem. Rev.*, 2007, **107**, 2891–2959.
4 A. Linsebigler, G. Lu and J. T. Yates, *Chem. Rev.*, 1995, **95**, 735–758.
5 X. Xu, G. R. Yang, J. Liang, S. J. Ding, C. L. Tang, H. H. Yang, W. Yan, G. D. Yang and D. M. Yu, *J. Mater. Chem. A*, 2014, **2**, 116–122.
6 S. Sakthivel and H. Kisch, *Angew. Chem., Int. Ed.*, 2003, **42**, 4908–4911.
7 L. Zhang, D. W. Jing, X. L. She, H. W. Liu, D. J. Yang, Y. Lu, J. Li, Z. F. Zheng and L. J. Guo, *J. Mater. Chem. A*, 2014, **2**, 2071–2078.
8 Y. P. Zhang, L. F. Fei, X. D. Jiang, C. X. Pan and Y. Wang, *J. Am. Ceram. Soc.*, 2011, **94**, 4157–4161.
9 L. W. Zhang, H. B. Fu and Y. F. Zhu, *Adv. Funct. Mater.*, 2008, **18**, 2180–2189.
10 L. Zhao, X. F. Chen, X. C. Wang, Y. J. Zhang, W. Wei, Y. H. Sun, M. Antonietti and M. M. Titirici, *Adv. Mater.*, 2010, **22**, 3317–3321.
11 X. Q. An, J. C. Yu, Y. Wang, Y. M. Hu, X. L. Yu and G. J. Zhang, *J. Mater. Chem.*, 2012, **22**, 8525–8531.
12 H. C. Zhang, H. Huang, H. Ming, H. T. Li, L. L. Zhang, Y. Liu and Z. H. Kang, *J. Mater. Chem.*, 2012, **22**, 10501–10506.
13 H. Ming, Z. Ma, Y. Liu, K. M. Pan, H. Yu, F. Wang and Z. H. Kang, *Dalton Trans.*, 2012, **41**, 9526–9531.
14 H. T. Li, X. D. H, Z. H. Kang, H. Huang, Y. Liu, J. L. Liu, S. Y. Lian, C. H. A. Tsang, X. B. Yang and S. T. Lee, *Angew. Chem., Int. Ed.*, 2010, **49**, 4430–4434.
15 H. T. Li, R. H. Liu, Y. Liu, H. Huang, H. Yu, H. Ming, S. Y. Lian, S. T. Lee and Z. H. Kang, *J. Mater. Chem.*, 2012, **22**, 17470–17475.
16 N. Zhang, Y. H. Zhang and Y. J. Xu, *Nanoscale*, 2012, **4**, 5792–5813.
17 L. Han, P. Wang and S. J. Dong, *Nanoscale*, 2012, **4**, 5814–5825.
18 H. Zhang, X. J. Lv, Y. M. Li, Y. Wang and J. H. Li, *ACS Nano*, 2010, **4**, 380–386.
19 P. Zhang, C. L. Shao, Z. Y. Zhang, M. Y. Zhang, J. B. Mu, Z. C. Guo and Y. C. Liu, *Nanoscale*, 2011, **3**, 2943–2949.
20 P. Zhang, C. L. Shao, Z. Y. Zhang, M. Y. Zhang, J. B. Mu, Z. C. Guo, Y. Y. Sun and Y. C. Liu, *J. Mater. Chem.*, 2011, **21**, 17746–17753.
21 P. Carniti, A. Gervasini, S. Biella and A. Auroux, *Catal. Today*, 2006, **118**, 373–378.
22 X. Y. Chen, T. Yu, X. X. Fan, H. T. Zhang, Z. S. Li, J. H. Ye and Z. G. Zou, *Appl. Surf. Sci.*, 2007, **253**, 8500–8506.
23 A. G. S. Prado, L. B. Bolzon, C. P. Pedroso, A. O. Moura and L. L. Costa, *Appl. Catal., B*, 2008, **82**, 219–224.
24 H. Kominami, K. Oki, M. Kohno, S. Onoue, Y. Kera and B. Ohtani, *J. Mater. Chem.*, 2001, **11**, 604–609.
25 T. Ohuchi, T. Miyatake, Y. Hitomi and T. Tanaka, *Catal. Today*, 2007, **120**, 233–239.
26 H. Matsui, K. Kira, S. Karuppuchamy and M. Yoshihara, *Curr. Appl. Phys.*, 2009, **9**, 592–597.
27 A. Esteves, L. C. A. Oliveira, T. C. Ramalho, M. Goncalves, A. S. Anastacio and H. W. P. Carvalho, *Catal. Commun.*, 2008, **10**, 330–332.
28 S. X. Ge, H. M. Jia, H. X. Zhao, Z. Zheng and L. Z. Zhang, *J. Mater. Chem.*, 2010, **20**, 3052–3058.
29 S. H. Zhan, D. R. Chen, X. L. Jiao and C. H. Ta, *J. Phys. Chem. B*, 2006, **110**, 11199–11204.

30 Z. Liu, D. D. Sun, P. Guo and J. O. Leckie, *Nano Lett.*, 2007, **7**, 1081–1085.
31 D. Li and Y. N. Xia, *Adv. Mater.*, 2004, **16**, 1151–1170.
32 A. Greiner and J. H. Wendorff, *Angew. Chem., Int. Ed.*, 2007, **46**, 5670–5703.
33 C. Berger, Z. M. Song, X. B. Li, X. Wu, N. Brown, C. Naud, D. Mayou, T. B. Li, J. Hass, A. N. Marchenkov, E. H. Conrad, P. N. First and W. A. de Heer, *Science*, 2006, **312**, 1191–1196.
34 S. Stankovich, D. A. Dikin, G. H. B. Dommett, K. M. Kohlhaas, E. J. Zimney, E. A. Stach, R. D. Piner, S. T. Nguyen and R. S. Ruoff, *Nature*, 2006, **442**, 282–286.
35 S. S. Qi, R. Z. Zuo, Y. Liu and Y. Wang, *Mater. Res. Bull.*, 2013, **48**, 1213–1217.
36 Y. Guo, H. S. Wang, C. L. He, L. J. Qiu and X. B. Cao, *Langmuir*, 2009, **25**, 4678–4684.
37 Y. W. Son, M. L. Cohen and S. G. Louie, *Phys. Rev. Lett.*, 2006, **97**, 216803.
38 M. Y. Han, B. Özyilmaz, Y. B. Zhang and P. Kim, *Phys. Rev. Lett.*, 2007, **98**, 206805.
39 D. L. Zhao, G. D. Sheng, C. L. Chen and X. K. Wang, *Appl. Catal., B*, 2012, **111–112**, 303–308.
40 N. Zhang, Y. H. Zhang, X. Y. Pan, X. Z. Fu, S. Q. Liu and Y. J. Xu, *J. Phys. Chem. C*, 2011, **115**, 23501–23511.
41 S. An, B. N. Joshi, M. W. Lee, N. Y. Kim and S. S. Yoon, *Appl. Surf. Sci.*, 2014, **294**, 24–28.
42 X. Q. An, X. L. Yu, J. C. Yu and G. J. Zhang, *J. Mater. Chem. A*, 2013, **1**, 5158–5164.
43 B. J. Li and H. Q. Cao, *J. Mater. Chem.*, 2011, **21**, 3346–3349.
44 J. G. Hou, S. Q. Jiao, H. M. Zhu and R. V. Kumar, *CrystEngComm*, 2011, **13**, 4735–4740.
45 S. D. Zhuang, X. Y. Xu, B. Feng, J. G. Hu, Y. Pang, G. Zhou, L. Tong and Y. X. Zhou, *ACS Appl. Mater. Interfaces*, 2014, **6**, 613–621.
46 Y. Q. Dai, Y. B. Sun, J. Yao, D. D. Lin, Y. M. Wang, H. Long, X. T. Wang, B. P. Lin, T. Y. H. Zeng and Y. S. Sun, *J. Mater. Chem. A*, 2014, **2**, 1060–1067.